*B*1-to-*B*8 structural phase transition in MnO under pressure: Comparison of all-electron and pseudopotential approaches

Jindřich Kolorenč* and Lubos Mitas
Department of Physics, North Carolina State University, Raleigh, North Carolina 27695, USA
(Received 10 August 2006; revised manuscript received 9 April 2007; published 22 June 2007)

We employ the density-functional theory to study a structural transition of MnO from *B*1 (rocksalt) to *B*8 (NiAs) structures that was observed experimentally at pressures around 100 GPa. We utilize all-electron description as well as norm-conserving pseudopotentials and demonstrate that these two approaches can significantly differ in quantitative predictions. We explicitly show that even small-core pseudopotentials exhibit transferability inaccuracies for quantities sensitive to the energy differences between high- and low-spin polarizations of valence electrons.

DOI: 10.1103/PhysRevB.75.235118 PACS number(s): 72.80.Ga, 71.15.−m, 71.20.−b, 64.30.+t

I. INTRODUCTION

Transition-metal oxides have received considerable attention from condensed matter physicists in the past several decades. One of the reasons for such an elevated interest is that the standard band theory methods, such as the density-functional theory (DFT) represented by the local-density approximation (LDA) or by its semilocal generalization [generalized gradient approximation (GGA)], do not satisfactorily describe these materials. For example, the LDA and GGA predict incorrect equilibrium crystal structure for FeO.[1,2] In the case of equilibrium properties of MnO, these approximations perform reasonably well as was shown by several groups.[3,4] The source of deficiencies of simple band theories is agreed to be the underestimation of correlations among 3*d* electrons. Improved accounting of these correlations is needed to adequately capture the Mott insulating mechanism and the competing charge-transfer effects.

Several methods have been devised to resolve the issue of strongly correlated electrons, such as GW, LDA+*U*, self-interaction correction, or hybrid exchange-correlation functionals that combine local exchange from LDA or GGA with nonlocal Fock exchange. Performance of several of these approaches has recently been thoroughly compared in Ref. 5, using the pressure-induced high-spin to low-spin transition[6] in MnO as a benchmark test. It turned out that although the current computational techniques work well for some aspects of the electronic structure (such as the equilibrium volume or the character of the ground state at ambient pressure), they are not quite dependable if one considers high-pressure properties of this material.

One of the goals of this paper is to provide additional benchmarks for the electronic structure of manganese oxide at high pressure, expanding thus the test set of Ref. 5. Our main message does not directly relate to the 3*d* electrons but to a rather surprising finding that the deep core states and the type of method used for their description can significantly influence certain properties generally considered to be related to the valence electrons only. An example of such a quantity is the critical pressure P_c for the pressure-induced transition from *B*1 (rocksalt) to *B*8 (NiAs) structure that has been reported recently.[7,8] This transition is accompanied by a collapse of the local magnetic moments of Mn atoms[8] as well as by electronic transition to a metallic state.[9]

Another key motivation for this study of core-valence interactions in crystalline MnO is our interest in applications of quantum Monte Carlo (QMC) techniques to transition-metal oxides and other materials containing strongly correlated electrons. The accurate representation of physical ions by norm-conserving pseudopotentials is essential for obtaining meaningful and predictive quantum Monte Carlo results, and it is therefore crucial to assess the accuracy and limits of such pseudopotential Hamiltonians. Ideally, one would compare the results of pseudopotential QMC with all-electron QMC. Unfortunately, such a route is prohibitively computationally expensive at present. We have therefore decided to carry out a careful study within the DFT, Hartree-Fock (HF) approximation, and a combination of these methods, since the accuracy of one-particle orbitals is important in QMC as mentioned below and explained elsewhere.[10,11] Similar problems were investigated in several density-functional studies (e.g., Refs. 12–15) and provided important signals that the choice of the methods and treatment of pseudopotentials can affect the final results.

Our study provides insights on several important and complementary directions. First, we employ Dirac-Fock pseudopotentials, which nominally should not require any additional corrections (such as the DFT nonlinear core correction as will be commented later on). The reason for this choice is that these pseudopotentials were designed to be accurate for correlated wave-function calculations and, in fact, several tests have been carried out within both post-Hartree-Fock (configuration interaction) and quantum Monte Carlo methods with quite satisfactory results.[10,11] Second, we wanted to quantify the pseudopotential vs all-electron differences within the DFT, HF, and hybrid functionals since our previous[10] (and current preliminary) calculations show that the hybrid functionals provide the most optimal one-particle orbitals, which minimize the fixed-node error in the quantum Monte Carlo method. The use of two independent codes and basis sets provides a solid computational framework for accurate benchmarking of these issues. In addition, study of high-pressure phase adds another important test, since the dramatic changes in electronic structure probe the pseudopotentials in the regime, for which their reliability cannot be taken for granted.

II. AMBIENT PRESSURE

Before we proceed with the investigation of the $B1$-to-$B8$ phase transition, we first concentrate on energy differences between various magnetic phases at ambient pressure. We apply the all-electron method side by side with the pseudopotential approach. For this purpose, we have modified the WIEN2K package[16] so that one can use either the original all-electron core solver or the norm-conserving pseudopotentials (PPs). The valence states are expanded in the linearized augmented plane wave (LAPW) basis (extended by local orbitals) in both cases. This allows for a systematic comparison of full cores with PPs, since the only point where such calculations differ is the treatment of the core electrons. Similar combination of LAPW and pseudopotentials was already used to look into some aspects of PP applications to transition metals.[13]

In order to minimize errors associated with partitioning core-valence correlations in pseudopotential calculations, we have chosen pseudopotentials with $3s$ and $3p$ states in the valence space, so that the eliminated core corresponded to the Ne atom. We tested two types of norm-conserving PPs constructed from Dirac-Fock atomic solutions. The first one, denoted as YN, is a soft pseudopotential generated using Troullier-Martins construction.[17] The second PP, labeled as STU, is the so-called energy-adjusted pseudopotential,[18] which has the $-Z_{eff}/r$ attractive ionic part retained.

In addition to performance of pseudopotentials, we were interested in the impact of exact exchange on electronic structure of manganese oxide. To this end, we have employed the CRYSTAL2003 code[19] that uses Gaussian-type atomic orbitals as a basis for one-particle wave functions. In the following, we refer to this method as linear combination of atomic orbitals (LCAO). The exact exchange was studied by means of two hybrid exchange-correlation functionals. We utilized B3LYP as well as somewhat simpler PBE0 functional. The later one is schematically written as

$$E_{xc}^{PBE0} = aE_x^{HF} + (1-a)E_x^{PBE} + E_c^{PBE}, \qquad (1)$$

where E_x^{PBE} and E_c^{PBE} are exchange and correlation parts of the Perdew-Burke-Ernzerhof (PBE)-GGA,[20] E_x^{HF} is the exact (Fock) exchange, and $a>0$. This type of hybrid mixing has the advantage that it directly relates to the PBE-GGA approximation employed in our LAPW calculations. We use a rather small value $a=1/10$ for the Fock mixing weight to account for the (nearly) metallic behavior at pressures we are going to investigate later. In the rest of the paper we abbreviate this functional as $PBE0_{10}$. With the standard choice of $a=1/4$,[21] we ran into serious difficulties in converging the Kohn-Sham equations when the lattice was compressed to the extent needed to reach the $B1$-to-$B8$ transition. Another alternative and possibly more sophisticated way around this problem is to employ a screened exchange instead of the full one.[5,22]

The outcome of the electronic structure methods introduced above is summarized in Table I, where we compare two electronic phases of MnO in the rocksalt structure at equilibrium lattice constant: the nonmagnetic (NM) state and the state with antiferromagnetic (AFM) ordering of adjacent Mn (111) planes, i.e., the so-called type-II antiferromagnet. The AFM phase represents the ambient pressure ground state.

TABLE I. Energy difference $\Delta=E_{\mathrm{AFM}}-E_{\mathrm{NM}}$ per MnO at lattice constant 4.43 Å together with local moments m formed on Mn atoms in the AFM phase. The disagreement between Δ^{all} and Δ^{PP} has opposite signs in PBE-GGA and HF calculations and is considerably reduced for hybrid functionals, especially for B3LYP. Note that there are slight inconsistencies between LAPW and LCAO local magnetic moments due to their different definitions. In the LCAO method, the projections onto all Gaussian basis functions centered on a given atom are considered, whereas within the LAPW only contributions from inside the relevant muffin-tin sphere are counted into the local moments. This makes the LAPW moments a little smaller than LCAO ones.

XC functional	Core	Δ (eV)	$\Delta^{all}-\Delta^{PP}$ (eV)	m (μ_B)
GGA, LAPW	All-electron	−2.29		4.23
	YN	−2.80	0.50	4.29
	STU	−2.94	0.65	4.32
GGA, LAPW, nonrelativistic	All-electron	−2.31		4.23
	YN	−2.78	0.47	4.29
	STU	−2.92	0.61	4.31
GGA, LCAO	All-electron	−2.39		4.59
	YN	−2.83	0.44	4.63
	STU	−2.96	0.57	4.64
$PBE0_{10}$, LCAO	All-electron	−3.50		4.70
	YN	−3.82	0.33	4.71
	STU	−3.91	0.41	4.71
B3LYP, LCAO	All-electron	−4.15		4.74
	YN	−4.24	0.09	4.74
	STU	−4.33	0.18	4.74
HF, LCAO	All-electron	−12.73		4.93
	YN	−12.55	−0.18	4.91
	STU	−12.18	−0.55	4.90

In the case of the LAPW method, the basis size and the density of k-point mesh were converged down to 1 or 2 mRy (~0.03 eV) in obtained total energies per MnO. The muffin-tin radii R_{MT} were chosen $2.11a_B$ for manganese and $1.86a_B$ for oxygen (a_B stands for Bohr radius). The cutoff energy for the interstitial plane-wave expansion was ≈23.4 Ry ($RK_{max}=9$). Local-orbital extensions were used for Mn s and p channels and O s channel to improve description of semicore states. The k-point sets consisted of 570 inequivalent points for the type-II AFM phase and 256 inequivalent points for the nonmagnetic and ferromagnetic (FM) phases. These numbers correspond to 5832 and 8000 points in the respective first Brillouin zones. The Gaussian basis set for the LCAO methods was chosen large enough to reproduce the (nonrelativistic) LAPW-GGA results (see Table I).

Since we utilized only small-core pseudopotentials, we expected only minor discrepancies between the all-electron

and PP calculations. However, this assumption turned out not to be entirely correct. The results listed in Table I show that both the *explicit presence of the core* and *the method which is employed* do matter. The difference between the all-electron and pseudopotential techniques varies from +0.6 eV/MnO within the PBE-GGA functional to −0.6 eV/MnO in the Hartree-Fock method combined with the STU PP. While contributions of this magnitude might not be always relevant, for the purpose of comparing energies of different magnetic phases or in high-pressure transitions, such a difference turns out to be very significant.

In addition to the antiferromagnetic and nonmagnetic *B*1 phases, we included into our investigation also the ferromagnetically ordered *B*1 structure. This time the energy difference $\Delta = E_{AFM} - E_{FM}$ stays virtually the same irrespective of the core treatment used. This indicates that the sensitivity of Δ to the description of the core electrons is related to the difference in magnetic moments of the two involved states—the local moments in FM and AFM phases are almost identical, approximately $4.5\mu_B$ (see Table I), whereas they are, by definition, zero in the NM state. More detailed evidence pointing in this direction is presented within the high-pressure study below.

Several comparisons of all-electron and small-core pseudopotential data can be found in the literature in connection with the so-called nonlinear core correction (NLCC).[12] LDA studies of 3*d* atoms[23] and transition-metal-bearing diatomic molecules[24] show that without the NLCC the errors in energetics, associated with small-core pseudopotentials, are generally of the order of tenths of eV, which is in agreement with our observations made in solids. The nonlinear core correction is demonstrated to be capable of removing a large portion of these errors.[23,24]

We have decided not to include the NLCC in our study for the following reason. The NLCC concept, correcting for linearization of core-valence correlations inherent to the standard norm-conserving pseudopotential technique, is not systematically transferable to methods using exact exchange, i.e., to hybrid exchange-correlation functionals, or to many-body methods such as quantum Monte Carlo. For these approaches, it is therefore important to assess how accurately the actual pseudopotential Hamiltonian represents the physical ion. Indeed, our study is a test of whether this appears to be true for a variety of magnetic states, range of pressures, and different methods. In the next section we provide additional benchmarks for MnO molecule and Mn atom, which clearly delineate the consistency of the PPs used and also suggest the reason for the discrepancies we found. Although the discussion of pseudopotential constructions is out of the scope of this paper, we just note that the core-valence partitioning is more straightforward within the Dirac-Fock approximation than within the DFT due to the rather complicated nonlinear dependence of the DFT exchange-correlation functional on the density. In fact, one set of the Dirac-Fock pseudopotentials we employed has been used in high-accuracy correlated calculations by quantum-chemical methods in a routine manner without additional corrections and with satisfactory results for equilibrium properties of molecular systems.[10,11,25]

TABLE II. Dissociation energy D_e of MnO molecule at a bond length of 1.64 Å calculated with restricted open shell (ROHF) and unrestricted (UHF) Hartree-Fock methods. Both the molecule and Mn atom are in a high-spin configuration with spin multiplicity 6.

Method	Core	D_e (eV)	$D_e^{all} - D_e^{PP}$ (eV)
ROHF	All-electron	−0.86	
	YN	−0.85	−0.01
	STU	−0.94	0.08
UHF	All-electron	0.69	
	YN	0.66	0.03
	STU	0.60	0.09

III. TESTING THE PSEUDOPOTENTIALS IN Mn ATOM AND MnO MOLECULE

The results presented in the preceding paragraph might appear somewhat surprising, since very small errors generated by small-core PPs have been observed in isolated atoms.[10,18] In particular, our Hartree-Fock tests of atomic $s \rightarrow d$ transfer energies, i.e., differences between high-spin and low-spin states in the isolated atom (not explicitly shown), turned out the same regardless of whether all-electron or pseudopotential Hamiltonian has been employed. In addition, our previous calculations within high-accuracy quantum Monte Carlo reproduced the experimental $s \rightarrow d$ transfer energy within 0.1 eV.[10] This suggests that the norm-conserving Dirac-Fock construction provides accurate PP Hamiltonian, which represents the physical ion within both the mean-field and correlated many-body methods with accuracy better than 0.1 eV. A question that arises is where is the origin of the discrepancies reported in the previous section. Is it something related solely to the solid-state environment or can it be detected as soon as chemical bonds are formed? The LDA study of molecules containing transition-metal atoms[24] suggests that the second statement is indeed true. To verify this we performed several Hartree-Fock calculations to demonstrate that such a conclusion is not only LDA specific.

Tables II and III show results obtained using the GAMESS

TABLE III. Energy difference $\Delta = E_{ls} - E_{hs}$ between high-spin ($\sigma^1\delta^1\bar{\delta}^1\pi^1\bar{\pi}^1$, multiplicity 6) and low-spin ($\sigma^1\delta^2\bar{\delta}^2$, multiplicity 2) configurations of MnO molecule calculated with Hartree-Fock methods. Bond length is 1.64 Å as in Table II.

Method	Core	Δ (eV)	$\Delta^{all} - \Delta^{PP}$ (eV)
E_{ls} with ROHF, E_{hs} with ROHF	All-electron	6.59	
	YN	6.69	−0.10
	STU	6.76	−0.17
E_{ls} with ROHF, E_{hs} with UHF	All-electron	8.42	
	YN	8.50	−0.08
	STU	8.61	−0.19

code[26] with large uncontracted basis sets for pseudoatoms and with natural atomic orbitals[27,28] for all-electron atoms. Whenever only same spin states are involved, as is the case of the dissociation energy D_e (Table II) of the ground state of MnO molecule, the all-electron and pseudopotential results agree quite well. Especially when YN pseudopotential is used, the difference $D_e^{all}-D_e^{PP}$ falls quite clearly below the resolution of the basis sets employed. In addition, tests done with highly correlated multideterminant Slater-Jastrow trial wave functions and with fixed-node diffusion Monte Carlo reproduced the experimental binding energy within 0.1 eV.[11] Therefore, even cohesive properties of the PP Hamiltonian look correct both within mean-field and many-body correlated methods.

A small but visible inconsistency between all-electron and pseudopotential approaches suddenly appears if one considers a *high-spin to low-spin transition in the molecule* (Table III). Electronic configurations are $\sigma^1\delta^1\bar{\delta}^1\pi^1\bar{\pi}^1$ for the high-spin state and $\sigma^1\delta^2\bar{\delta}^2$ for the low-spin state. Comparison of quantities $\Delta^{all}-\Delta^{PP}$ between Tables I and III shows that the discrepancies in the solid are almost three times larger than in the molecule. This is understandable since the Mn bonding in solid is enhanced by the octahedral arrangement of the oxygen atoms. Trying to estimate how much stronger this effect would be from the size of cohesions, one finds that the ratio of (experimental) binding energies[29,30] of the two systems is 9.5 eV/3.8 eV=2.5. The key question which therefore remains to be answered is the following: Where is this effect coming from? We believe that the bonding environment is the key consideration for resolving this issue. In an isolated atom the d electrons have freedom to expand away from the nucleus and, indeed, one finds that the atomic d orbitals for low-spin states are very diffuse. In the presence of chemical bond, say, in a molecule, such an expansion is not favorable, since bonding tends to localize the states even for doubly occupied d channels. In a solid this is even more pronounced as the Mn atom is encapsulated in the octahedron of oxygens. This enhances the amount of charge in the d states inside the core. The cause for the spin-related discrepancies then becomes apparent—it is the bonding (or chemical) "pressure".

IV. SOLID AT HIGH PRESSURES: GGA

In order to examine the high-pressure behavior of MnO, namely, the $B1$-to-$B8$ transition, we have carried out a series of LAPW PBE-GGA calculations[41] for the type-II antiferromagnetic phase in the $B1$ structure and for the $B8$ structure with ferromagnetic as well as antiferromagnetic ordering of hexagonal Mn planes.[42] The critical pressure P_c and volume change at the $B1$-to-$B8$ transition are listed on the first two lines of Table IV. The arrangement of local moments is found to change from AFM to FM across the transition. The choice of the magnetic ordering in the high-pressure phase is not well resolved, however, since the energy difference between $B8$ AFM and $B8$ FM phases at the relevant volumes is comparable to our 2 mRy precision estimate. The Fermi level lies in the gap between bands of the Kohn-Sham eigenvalues from ambient pressure all the way up to the transition

TABLE IV. Critical pressures for the $B1$ AFM to $B8$ FM phase transition as calculated with various methods. Also indicated are volumes (per formula unit) and the local magnetic moments on Mn atoms for both phases at the transition.

Method	P_c (GPa)	V_{B1} (Å^3)	V_{B8} (Å^3)	m_{B1} (μ_B)	m_{B8} (μ_B)
GGA, all-electron LAPW	43	18.15	15.76	3.8	2.3
GGA, YN LAPW	67	17.01	14.98	3.9	2.4
PBE0$_{10}$, all-electron LCAO	117	15.48	13.71	4.4	2.0
PBE0$_{10}$, YN LCAO	125	15.12	13.17	4.4	2.0

in the case of the $B1$ AFM phase, whereas it is located inside a band for both studied $B8$ phases above and also well below P_c. These qualitative features do not change if full cores or pseudopotentials are used. The variation in quantitative aspects is, on the other hand, quite sizable. For instance, the difference in the transition pressure P_c is as large as 25 GPa.

The GGA predictions are rather far from experimental P_c, around 100 GPa,[7–9] and from a nonmagnetic high-pressure phase[8] observed at room temperature (our calculations would support a paramagnetic phase at this temperature, at best). This is not surprising as the GGA is not expected to approximate the electronic structure of MnO very accurately. At the same time, the pressure $P_c=67$ GPa resulting from our PP calculations is in good agreement with results of Fang *et al.*,[31] who obtained $P_c\approx 60$ GPa with a plane-wave pseudopotential approach. The remaining few gigapascals might originate from differences between utilized pseudopotentials (e.g., ours are Ne core, theirs are Ar core) and from the full structure optimization performed in Ref. 31. For the sake of simplicity, we have neglected the rhombohedral distortion in the $B1$ AFM phase and have not optimized the c/a ratio in the $B8$ phases. Instead, we used a constant value $c/a=2.0$ consistent with the outcome of Ref. 31 and slightly smaller than $c/a\approx 2.1$ suggested by x-ray spectroscopy.[8]

Figures 1 and 2 relate the discrepancy between the two distinct core electron treatments to magnetic moments formed on manganese atoms. The quantity we used to measure the difference between all-electron and pseudopotential total energies is defined as

$$\varepsilon(V)=[E^{all}(V)-E_{B1}^{all}(V_{B1}^{(0)})]-[E^{PP}(V)-E_{B1}^{PP}(V_{B1}^{(0)})], \quad (2)$$

where $V_{B1}^{(0)}$ stands for a reference volume. We use $V_{B1}^{(0)}=21.7$ Å^3/MnO, i.e., the maximum volume studied for the $B1$ phase. Note that Figs. 1 and 2 do not change if we choose the reference point to be in the $B8$ phase at the maximum volume we consider ($V_{B8}^{(0)}=23.4$ Å^3). The difference in the respective reference energies is only

$$[E_{B1}^{all}(V_{B1}^{(0)})-E_{B1}^{PP}(V_{B1}^{(0)})]-[E_{B8}^{all}(V_{B8}^{(0)})-E_{B8}^{PP}(V_{B8}^{(0)})]\approx 0.005 \text{ eV},$$

which falls below the resolution we claim here. The equivalence of these two reference points is in concord with our findings presented in the preceding sections, since the corresponding local magnetic moments on Mn atoms are essentially the same, namely,

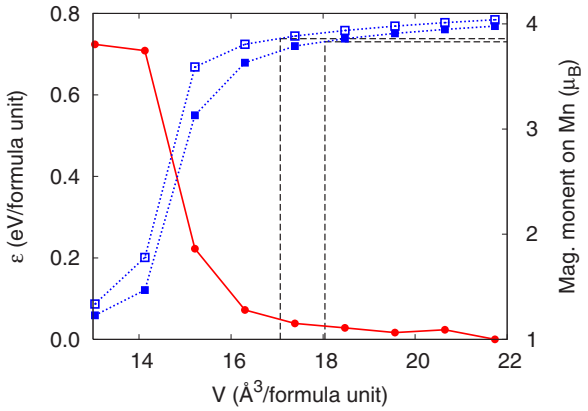

FIG. 1. (Color online) Difference between all-electron and pseudopotential total energies [Eq. (2)], as calculated for the *B*1 AFM structure within LAPW PBE-GGA method (bullets). Also shown is magnetic moment on the Mn atom with all-electron core (full squares) and YN pseudopotential (empty squares). The slight enhancement of local moments when pseudopotentials are introduced, visible also in Tables I and IV, is consistent with other reports (Refs. 13 and 32). Volumes at the transition to the *B*8 FM phase are indicated as well.

$$m_{B1}^{all}(V_{B1}^{(0)}) = 4.01\mu_B,$$

$$m_{B8}^{all}(V_{B8}^{(0)}) = 3.98\mu_B.$$

In the rocksalt structure, the difference ε as a function of volume remains almost constant as long as the spin polarization does not change, and jumps up at the high-spin to low-spin transition (Fig. 1). Consequently, the all-electron and pseudopotential predictions for thermodynamically relevant properties, such as the equation of state $P(V) = -\partial E/\partial V$, coincide until the spin transition is reached and start to diverge afterward. In the *B*8 phase, the magnetic moment decreases gradually with volume compression and this reduction is accompanied with a gradual change of the difference ε that reaches an appreciable value at the point of the phase transition (see Fig. 2). The fact that the variation of the total energy difference ε apparently follows the evolution of spin polarization suggests that some type of spin-dependent pseudopotentials, possibly those introduced in Ref. 33, might bring the all-electron and pseudopotential results closer together.

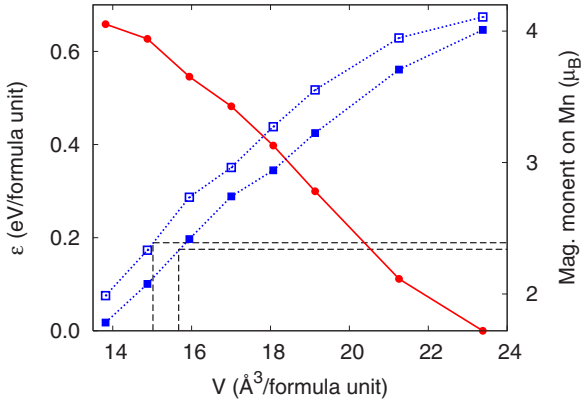

FIG. 2. (Color online) Same quantities as in Fig. 1 but for *B*8 FM structure.

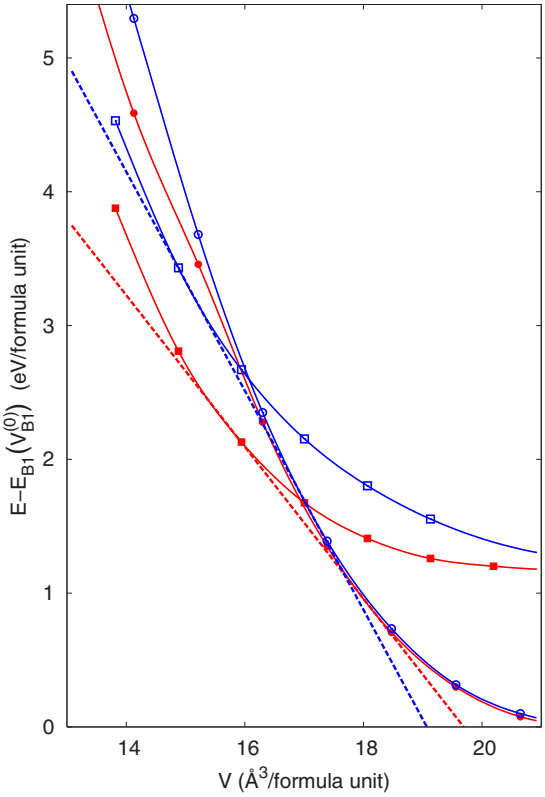

FIG. 3. (Color online) Total energies of *B*1 AFM (circles) and *B*8 FM (squares) phases as they depend on the volume for the LAPW PBE-GGA method. Both all-electron (filled symbols) and pseudopotential (empty symbols) data are shown together with the corresponding double tangents illustrating the respective transition pressures.

Finally, Fig. 3 provides a graphical insight on how the aforementioned variations in the $E(V)$ curves give rise to the 25 GPa inconsistency between the transition pressures P_c determined within all-electron and pseudopotential frameworks.

V. SOLID AT HIGH PRESSURES: HYBRID FUNCTIONAL

To evaluate how the exact exchange influences the critical pressure of the *B*1-to-*B*8 transition, we repeated the calculations with the PBE0$_{10}$ functional as shown on the last two lines of Table IV. We can see that already a small admixture of exact exchange moves the critical pressure P_c way above the GGA prediction, just a little higher than experimentally observed. Corresponding volumes of the phases above and below the transition are also very close to the experimental results.[8] We would like to emphasize, however, that this study is targeted on methodology rather than on precise comparison with experiments since the latter's goal would certainly require detailed geometry optimizations. The overall picture of the transition within PBE0$_{10}$ stays the same as with the GGA: the rocksalt phase is an insulator; the *B*8

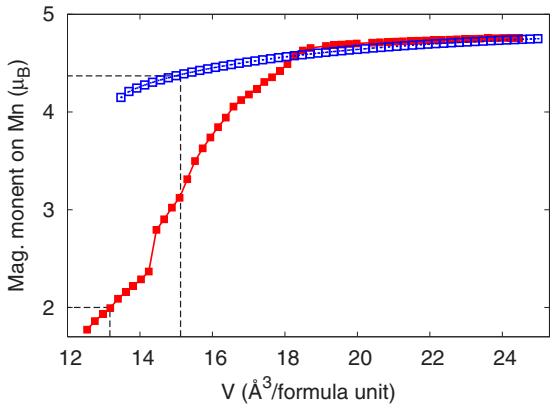

FIG. 4. (Color online) Magnetic moment on Mn atom in $B1$ AFM (empty squares) and $B8$ FM (full squares) phases as calculated using the $PBE0_{10}$ functional. Values are taken from YN PP calculation; corresponding all-electron data are virtually indistinguishable. Transition volumes are shown as well. The small skip around $V=14.4$ Å^3 is related to a more rapid transfer of occupation between the majority and minority bands that takes place at this volume. It occurs both in all-electron and pseudopotential data, and therefore it has no impact on the subject discussed in this study. No such skip is observed in the $B8$ AFM phase.

phase is a metal. The magnetic moments collapse from $4.4\mu_B$ to $2.0\mu_B$ as the MnO is compressed across the transition. The evolution of the magnetic moments with decreasing volume is shown in Fig. 4. The tendency of the Fock exchange toward electron localization is clearly visible: the decrease in moments is delayed to a lower volume in both $B1$ and $B8$ phases as compared to the GGA results displayed in Figs. 1 and 2. In the rocksalt structure, we actually see no high-spin to low-spin transition in the interval of examined volumes.

The discrepancy between all-electron and pseudopotential approaches is greatly reduced when a hybrid functional is used. Following the discussion of the GGA results, one might expect that this reduction is accompanied by limited spin changes. However, Fig. 4 demonstrates that this is not the case, and therefore, we conclude that the core treated by $PBE0_{10}$ is more inert and is less sensitive to changes of the local moment formed by valence electrons.

VI. CONCLUSIONS

Our findings complement several other reports found in the literature indicating that application of pseudopotential-based techniques to transition metals and their compounds is a delicate task.[14] In particular, we mention discrepancies in magnetic properties of the vanadium surface[34–36] or inconsistencies in predictions of the ground state of Ce_2O_3 (Refs. 37 and 38) found between pseudopotential and all-electron methods. In these studies, however, the large-core (Ar) PPs were utilized. The difficulties with pseudopotentials are then attributed to the semicore $3s$ and $3p$ states that have too large overlap with the valence $4s$ and $3d$ electrons to be accurately represented by a "rigid core". At the same time, the semicore states are usually too localized to be efficiently included in the valence space.[43] This type of argument, however, cannot explain the variations in the $B1$-to-$B8$ transition pressure presented in this paper, since we treat the $3s$ and $3p$ states as valence degrees of freedom. Our observations suggest that one should carefully examine transferability of pseudopotentials between different spin states even in the case of small-core PPs, especially if the phenomena under investigation involve variations in local magnetic moments.

Overall implications of our results are rather straightforward to explain. The $3d$ states have no counterparts of the same symmetry in the core, and therefore, an appreciable amount of the d charge density is localized in the core region. Consequently, changes in the local moments can influence the core states and vice versa. As we have verified, this is not detectable in isolated atoms, where the all-electron and pseudopotential results agree very well, nor in equilibrium ground-state cohesion energies, which do not involve dramatic changes in the local moment on the Mn atom. This is true not only for the mean-field methods employed in this study, but also for highly accurate quantum Monte Carlo tests done previously.[10,11] These results suggest that the PP Hamiltonian is consistent and accurate. The discrepancy appears and becomes visible when the *high-spin* to *low-spin differences* become involved in bonds. The localization of the d states due to the chemical environment pushes a larger fraction of the charge into the core and inaccuracies of various methods become more pronounced. The direction of the biases, which we found, is also not very difficult to understand. The LDA and GGA functionals are well known to incline toward smoother and more homogeneous densities with exaggerated softening of electron-electron repulsion. On the opposite side is the Hartree-Fock method, which tends to localize the states since that enhances the exchange contributions (the only mechanism through which HF can decrease the energy). The key point is that these biases affect *all degrees of freedom* of the given system, including, in all-electron calculations, also the core states. Therefore, the cores are "softened" in the LDA and GGA approaches and "tightened" in the HF approximation. In the PP case, the core is rigid and hence the bias from core states is absent. Finally, these results could be of interest not only for high-pressure solids but also for other transition-metal systems with significant magnetic moment changes such as biomolecular reaction centers or catalysis.

ACKNOWLEDGMENTS

We acknowledge support by NSF DMR-0121361 and EAR-0530110 grants. We would like to thank P. Blaha for his kind consent to modify the WIEN2K code.

*On leave from the Institute of Physics, Academy of Sciences of the Czech Republic, Na Slovance 2, CZ-18221 Praha 8, Czech Republic.

[1] I. I. Mazin, Y. Fei, R. Dawns, and R. Cohen, Am. Mineral. **83**, 451 (1998).

[2] Z. Fang, K. Terakura, H. Sawada, T. Miyazaki, and I. Solovyev, Phys. Rev. Lett. **81**, 1027 (1998).

[3] J. E. Pask, D. J. Singh, I. I. Mazin, C. S. Hellberg, and J. Kortus, Phys. Rev. B **64**, 024403 (2001).

[4] K. Terakura, T. Oguchi, A. R. Williams, and J. Kübler, Phys. Rev. B **30**, 4734 (1984).

[5] D. Kasinathan, J. Kuneš, K. Koepernik, C. V. Diaconu, R. L. Martin, I. Prodan, G. E. Scuseria, N. Spaldin, L. Petit, T. C. Schulthess, and W. E. Pickett, arXiv:cond-mat/0605430 (unpublished).

[6] R. E. Cohen, I. I. Mazin, and D. G. Isaak, Science **275**, 654 (1997).

[7] T. Kondo, T. Yagi, Y. Syono, Y. Noguchi, T. Atou, T. Kikegawa, and O. Shimomura, J. Appl. Phys. **87**, 4153 (2000).

[8] C. S. Yoo, B. Maddox, J.-H. P. Klepeis, V. Iota, W. Evans, A. McMahan, M. Y. Hu, P. Chow, M. Somayazulu, D. Hausermann, R. T. Scalettar, and W. E. Pickett, Phys. Rev. Lett. **94**, 115502 (2005).

[9] J. R. Patterson, C. M. Aracne, D. D. Jackson, V. Malba, S. T. Weir, P. A. Baker, and Y. K. Vohra, Phys. Rev. B **69**, 220101(R) (2004).

[10] L. Wagner and L. Mitas, Chem. Phys. Lett. **370**, 412 (2003).

[11] L. K. Wagner and L. Mitas, J. Chem. Phys. **126**, 034105 (2007).

[12] S. G. Louie, S. Froyen, and M. L. Cohen, Phys. Rev. B **26**, 1738 (1982).

[13] J.-H. Cho and M. Scheffler, Phys. Rev. B **53**, 10685 (1996).

[14] G. Kresse and D. Joubert, Phys. Rev. B **59**, 1758 (1999).

[15] A. Kiejna, G. Kresse, J. Rogal, A. De Sarkar, K. Reuter, and M. Scheffler, Phys. Rev. B **73**, 035404 (2006).

[16] P. Blaha, K. Schwarz, G. K. H. Madsen, D. Kvasnicka, and J. Luitz, WIEN2K, an augmented plane wave+local orbitals program for calculating crystal properties, Techn. Universität Wien, Austria, 2001.

[17] Y. Lee (private communication); see also Y. Lee, P. R. C. Kent, M. D. Towler, R. J. Needs, and G. Rajagopal, Phys. Rev. B **62**, 13347 (2000) for large-core version of these pseudopotentials.

[18] M. Dolg, U. Wedig, H. Stoll, and H. Preuss, J. Chem. Phys. **86**, 866 (1987).

[19] V. Saunders, R. Dovesi, C. Roetti, R. Orlando, C. M. Zicovich-Wilson, N. M. Harrison, K. Doll, B. Civalleri, I. Bush, P. D'Arco, and M. Llunell, *CRYSTAL2003 User's Manual* (University of Torino, Torino, 2003).

[20] J. P. Perdew, K. Burke, and M. Ernzerhof, Phys. Rev. Lett. **77**, 3865 (1996).

[21] J. P. Perdew, M. Ernzerhof, and K. Burke, J. Chem. Phys. **105**, 9982 (1996).

[22] J. Heyd, G. E. Scuseria, and M. Ernzerhof, J. Chem. Phys. **118**, 8207 (2003).

[23] D. Porezag, M. R. Pederson, and A. Y. Liu, Phys. Rev. B **60**, 14132 (1999).

[24] E. Engel, A. Höck, and S. Varga, Phys. Rev. B **63**, 125121 (2001).

[25] M. Dolg, U. Wedig, H. Stoll, and H. Preuss, J. Chem. Phys. **86**, 2123 (1987).

[26] M. W. Schmidt, K. K. Baldridge, J. A. Boatz, S. T. Elbert, M. S. Gordon, J. H. Jensen, S. Koseki, N. Matsunaga, K. A. Nguyen, S. J. Su, T. L. Windus, M. Dupuis, and J. A. Montgomery, J. Comput. Chem. **14**, 1347 (1993).

[27] P.-O. Widmark, P. Malmqvist, and B. O. Roos, Theor. Chim. Acta **77**, 291 (1990).

[28] R. Pou-Amérigo, M. Merchán, I. Nebot-Gil, P.-O. Widmark, and B. O. Roos, Theor. Chim. Acta **92**, 149 (1995).

[29] I. Barin, *Thermochemical Data of Pure Substances*, 2nd ed. (VCH, Weinheim, 1993).

[30] S. Smoes and J. Drowart, High. Temp. Sci. **17**, 31 (1984).

[31] Z. Fang, I. V. Solovyev, H. Sawada, and K. Terakura, Phys. Rev. B **59**, 762 (1999).

[32] V. Cocula, F. Starrost, S. C. Watson, and E. A. Carter, J. Chem. Phys. **119**, 7659 (2003).

[33] S. C. Watson and E. A. Carter, Phys. Rev. B **58**, R13309 (1998).

[34] I. G. Batyrev, J.-H. Cho, and L. Kleinman, Phys. Rev. B **63**, 172420 (2001).

[35] G. Kresse, W. Bergermayer, and R. Podloucky, Phys. Rev. B **66**, 146401 (2002).

[36] V. Cocula and E. A. Carter, Phys. Rev. B **69**, 052404 (2004).

[37] G. Kresse, P. Blaha, J. L. F. Da Silva, and M. V. Ganduglia-Pirovano, Phys. Rev. B **72**, 237101 (2005).

[38] S. Fabris, S. de Gironcoli, S. Baroni, G. Vicario, and G. Balducci, Phys. Rev. B **72**, 237102 (2005).

[39] D. Vanderbilt, Phys. Rev. B **41**, 7892 (1990).

[40] P. E. Blöchl, Phys. Rev. B **50**, 17953 (1994).

[41] The muffin-tin radii R_{MT} were set to $1.81a_B$ for Mn atom and $1.6a_B$ for oxygen, and were held constant for all volumes. This choice represents almost touching spheres for the smallest studied volume. Plane-wave cutoff was 31.6 Ry (RK_{max}=9). The k-point set for the $B1$ AFM phase was the same as in our ambient pressure calculations; for the $B8$ phases, we used 260 inequivalent points that corresponds to 4356 points in the first Brillouin zone.

[42] In the $B8$ phases, the Mn atoms occupy the Ni sites and oxygen atoms sit at the As sites.

[43] The problem of a large (plane-wave) cutoff required by localized semicore states can be successfully overcome within alternative frozen-core techniques such as ultrasoft pseudopotentials (Ref. 39) or the projector augmented-wave method (Refs. 14 and 40).